International Journal of Hydrogen Energy xxx (xxxx) xxx

Contents lists available at ScienceDirect

International Journal of Hydrogen Energy

journal homepage: www.elsevier.com/locate/he

Electrochemical behavior of Pt nano-particles dispersed on Cu/Ni electrode in alkaline environment

Serap Toprak Döşlü [a,b,*], Ali Döner [c]

[a] Mardin Artuklu University, Faculty of Health Sciences, Department of Nutrition and Dietetics, 47100, Mardin, Turkey
[b] Mardin Artuklu University, Central Research Laboratory, TR, 47100, Mardin, Turkey
[c] Gaziantep Islam Science and Technology University, Faculty of Engineering and Natural Sciences, Department of Basic Sciences, Gaziantep, 27010, Turkey

ARTICLE INFO

Handling Editor: Ibrahim Dincer

Keywords:
Hydrogen evolution reaction
Pt based electrocatalyst
Electrochemical properties

ABSTRACT

The development of a low-cost Pt-based electrocatalyst for industrial water splitting is important. In this study, to prepare cost-efficient Pt-based electrocatalyst for hydrogen evolution, Cu electrode is deposited with nickel (Cu/Ni) and this surface is modified with Pt nanoparticles by electrodeposition method (Cu/Ni–Pt). The surface properties of the produced electrocatalysts are studied via X-ray diffraction (XRD), scanning electron spectroscopy (SEM), energy dispersive X-ray analysis (EDX), transmission electron microscopy (TEM) and atomic force microscopy (AFM). Characterizations demonstrated that the coating is homogeneous and compact. Hydrogen evolution and corrosion behaviors of prepared electrode (Cu/Ni–Pt) are examined in 1.0 M KOH solution using cyclic voltammetry (CV) and cathodic and anodic current-potential curves, electrochemical impedance spectroscopy (EIS). Tafel slope is determined to be 133 mV dec^{-1} on Cu/Ni–Pt. Very high exchange current density (5.65 mA cm^{-2}) and very low charge transfer resistance (0.91 Ω cm^2 at 1.05 V vs RHE) are measured again on this electrocatalyst. High activity is due to intrinsic activity of Pt and synergistic interaction of Pt and Ni. Besides, Cu/Ni–Pt exhibits so stable structure over 4 h without any current densities decay as well as showing good corrosion performance after long-term immersion times and these properties make it possible electrocatalyst with high corrosion resistant and activity in the water electrolysis systems.

1. Introduction

Hydrogen production in water electrolysis is among the sustainable processes for future green technologies that have no carbon footprint and alleviate the aggravated pollution [1]. Water electrolyzers should be integrated with clean renewable power plants (solar, wind, hydro, etc.) that provide the necessary electricity for electrolyzers [2,3]. To produce hydrogen on a large scale, the activities of the electrocatalysts used at the cathode must be maximized. Platinum (Pt) at the top of the volcanic cathode is considered the agent of choice for catalyzing hydrogen evolution reactions under acidic or basic conditions [4,5]. The high price of platinum and its lack of abundance in nature limit its commercial use on a large scale. To overcome these disadvantages, many strategies have been developed. One strategy is to reduce the amount of platinum in the matrix by making a binary and ternary alloy. The other is to reduce the Pt particle size to increase the Pt dispersion [6,7] and thus the number of active Pt sites. This is because different metal atoms provide a favorable model for the synergism of platinum and other metals [1]. These strategies provide an increase in the utilization efficiency of Pt. Apart from the catalytic properties of the electrocatalysts, corrosion is a very important parameter for the lifetime of electrolyzers, as in all metal-containing industries. The catalysts used in electrolyzers should be corrosion resistant in the working environment and have high catalytic efficiency [8–10].

Combining the advantages of different catalytic materials into a new hybrid is an important but challenging task in the development of multifunctional electrodes for water splitting as a whole. In a study by Huang and colleagues, a strategy was developed to modify micro-platinum to create a dual-functional hybrid electrode of Pt@Co_3O_4/Ni foam for water division. It was found that the micro-Pt modified Co_3O_4 nanorod assembly had a synergistic effect with optimized water splitting and hydrogen recombination [11]. Mojabi and Sanjabi [12] reported the preparation of fractal Ni–Cu foam with palladium nanoparticles (Ni–Cu foam/Pd) and HER behavior of this catalyst was investigated in 1.0 M KOH solution. They stated that Ni–Cu foam/Pd had good electrocatalytic properties due to special morphology, fractal structure, very

* Corresponding author. Mardin Artuklu University, Faculty of Health Sciences, Department of Nutrition and Dietetics, 47100, Mardin, Turkey.
E-mail address: seraptoprak@artuklu.edu.tr (S.T. Döşlü).

https://doi.org/10.1016/j.ijhydene.2024.01.194
Received 29 September 2023; Received in revised form 8 January 2024; Accepted 17 January 2024
0360-3199/© 2024 Hydrogen Energy Publications LLC. Published by Elsevier Ltd. All rights reserved.

high surface area and presence of metals with desirable intrinsic properties. Chauhan et al. [13] studied the hydrogen evolution reaction on Pt/NiCo in 1.0 M KOH electrolyte. Their results showed that prepared electrocatalyst demonstrated excellent HER performance with a low overpotential of 48 mV at 10 mA cm^{-2}. High activity is related to Pt changing electronic structure of NiCo and increase the electrochemical surface area. Guo et al. [14] claimed that phosphated IrMo bimetallic cluster showed a highly efficient alkaline HER catalyst. This catalyst also exhibited a negligible decrease in overpotential after 27 h of testing, confirmed by no change in morphology.

In this work, platinum nanoparticles are produced on nickel-coated copper for the HER using one-step electrodeposition method that uses almost all Pt atoms. Pt nanoparticles modified with Cu/Ni showed higher activity for the HER compared to Cu/Ni, Cu/Ni–Pd and most literature data.

2. Materials and methods

Pt nanoparticles are deposited on the copper surface (0.283 cm^2) that is modified with nickel by electrodeposition. A nickel bath is used to prepare the Cu/Ni electrode. Composition of the nickel bath: 1.25 g H_3BO_3, 1.0 g $NiCl_2.6H_2O$, 28.072 g $NiSO_4.6H_2O$ (Total volume: 100 mL). The deposition time and current density are 2930 s and 50 mA cm^{-2}, respectively. Then Pt nanoparticles are deposited on this surface with a Pt bath consisting of 0.0352 g K_2PtCI_6, 2.95 g $Na_3C_6H_5O_7$, 0.37 g KCI (Total volume 50 mL). The deposition time and current density are 3600 s and 7.07 mA cm^{-2}, respectively. A palladium bath is used for palladium deposition (0.024 g $PdCI_2$, 2.94 g $Na_3C_6H_5O_7$, 0.37 g KCI (Total volume 50 mL), deposition time and current density are the same as for platinum). Before the deposition, the Cu electrode is polished with emery paper. Electrochemical techniques performed with three electrodes include cyclic voltammetry (CV), cathodic current-potential curves, electrochemical impedance spectroscopy (EIS) and anodic current-potential curves. Cyclic voltammograms are recorded in the potential window of the hydrogen and oxygen evolution ranges. EIS is plotted as Nyquist plots in the frequency range $1.0x10^5$ – 0.00398 Hz with an amplitude of 5 mV at different hydrogen evolution potentials (−1.05, −1.15 and −1.25 V (vs RHE)). Current-potential curves are plotted at a sampling rate of 5 mV s^{-1}, in the potential window of zero current potential and −1.6 V vs RHE for cathodic. At a sampling rate of 1 mV s^{-1}, in the potential window of open circuit potential (E_{ocp}) and 1.2 V vs RHE for anodic. The corrosion test at long immersion (24, 48, 72, 120 and 144 h) is performed using EIS in the frequency range of $1.0x10^5$ – 0.00398 Hz with an amplitude of 5 mV at E_{ocp}, as shown in Nyquist and Bode plots. Nyquist plots are fitted using the equivalent circuit model in Zview2 software. Prepared electrocatalysts are Cu, Cu/Ni, Cu/Ni–Pd and Cu/Ni–Pt. Chronoamperometry (CA) is performed for 4 h at −1.25 V vs RHE for durability. Furthermore, cyclic stability test is performed by CV technique at a scan rate of 50 mV s^{-1} in 1.0 M KOH until obtaining 400 cycles. CA and cyclic stability tests are carried out only on Cu/Ni–Pt. All experiments are carried out under room conditions, open to the atmosphere and in 1.0 M KOH solution. Pt foil (2 cm^2), Ag/AgCI (with KCI saturated) and prepared electrocatalysts are used in a three-electrode setup as counter, reference and working electrodes, respectively. All potential vs Ag/AgCI are converted to reversible hydrogen electrode (RHE) ($E_{RHE} = E_{Ag/AgCl} + 0.059\ pH + 0.197$ V [15]). All electrochemical experiments were performed using Gamry Instruments Potansiyostat&Galvanostat/ZRA/3000. For surface scans, JEOL JSM 6510 scanning electron microscope (SEM), rigaku ultima IV X-ray spectrometer (XRD), Jeol Jem 1010 transmission electron microscopy (TEM) and Park Systems XE-100 E atomic force microscopy (AFM) are used. Preparation of sample for TEM analysis is as follows: Ni–Pt coating is physically peeled off the Cu surface. The sample is made into small particles and is made ready for TEM analysis.

3. Results and discussion

3.1. Surface analysis

The analysis of the produced electrodes is done via XRD, SEM, EDX, EDX mapping, AFM and TEM procedure. Fig. 1 shows the SEM images, EDX spectrums of Cu (a) Cu/Ni (b,b'), Cu/Ni–Pd (c,c') and Cu/Ni–Pt (d, d'), EDX mapping and AFM images of Cu/Ni–Pt (e,f), respectively. Fig. 1a displays the abrasion marks of the sandpaper used to clean the surface of the copper electrode. Fig. 1b–d clearly show that densely stacked, homogeneously distributed layers have formed on the surface of the electrode. In Fig. 1c, the agglomerates of different size and distribution typical for Pd nanoparticles are clearly visible [16–18]. Based on the SEM images, it can be said that a homogeneous Ni, Ni–Pd and Ni–Pt coating has successfully formed on the entire surface. Nickel, copper, palladium and platinum peaks are clearly seen in related figures (Fig. 1b',c' and d'). In Fig. 1h, it is understood that Ni and Pt are distributed homogeneously on the surface and are present on the entire surface [19–21]. The EDX results showing the presence and composition of the metals on the copper surface coated for the production of an electrocatalyst are shown in Table 1. It is clearly seen that the amount of Cu has decreased considerably, meaning that the surface is almost completely closed. It was found that Pt in particular is quite rare (17.72 %) when compared to Ni (76.24 %). To support SEM images, AFM topography images are taken for Ni–Pt coating. These images are presented as 3D and 2D in Fig. 1e and f. While some hills form on the surface (3D), Pt nanoparticles appear in different size (3D and 2D). These particles are not visible in the SEM image of Ni–Pt coating (Fig. 1d). Surface roughness is found to be 114.27 nm. Size of the hills formed on the surface is almost 1 μm. TEM measurements are needed to observe whether nanoparticles form on the surface. TEM images of Cu/Ni–Pt electrocatalyst are showed in Fig. 2. As expected that light and dark areas with dentritic morphology appear on the surface (Fig. 2a). Average size of these particles is measured as 4.2 nm.

XRD images are performed to identify the crystal structure of the produced electrocatalysts. It shows the corresponding XRD patterns of the electrocatalysts in Fig. 3. The diffraction peaks at about, 43°, 50°, 62° and 89° correspond to (111), (002) (reference code: 98-005-3247), (020) (reference code: 98-024-8436) and (113) (reference code: 98-005-3757) of cubic Cu. The diffraction peaks belonging to cubic structure of Ni appearing at about 44°, 52° and 76° are assigned to (111), (002) and (022) of Ni (reference code: 98-007-6667). XRD peaks of Ni agree with the literature [22,23]. Besides, peaks of Cu at 50° and 89° are appeared. The corresponding diffraction peaks for Pt appear at almost 40°, 45°, 66° and 81° which characterize (111), (200), (220), (311) of the FFC Pt [24]. It also seen the peaks of Cu and Ni which are appeared at 89° for Cu and 76° for Ni. The diffraction peaks for face centered cubic (FCC) structure of Pd shown at almost 40°, 68°, 81°, and 86° belong to (111), (220), (311) and (222), respectively [25,26]. In addition to Pd peaks, Ni (52° and 76°) and Cu peaks (89°) are observed. The XRD pattern clearly shows that jolly good electrocatalyst film has formed on the surface. These results also agree well with the EDX spectrums and EDX mapping results. Appeared other peaks may be related to impurities.

3.2. Electrochemical behavior

All prepared electrocatalysts are characterized by CV and related voltammograms are given in Fig. 4. To compare, CV of Pt electrode is also recorded. In Fig. 4a, the characteristic peaks of platinum are clearly visible. These are hydrogen adsorption and desorption, double layer regions and PtO_x. CV of Cu is shown as inset in Fig. 4b [10]. The voltammogram shows three anodic peaks in the anodic region related to the conversions of Cu/Cu^{I}, Cu/Cu^{II} and Cu^{II}/Cu^{III}, and three cathodic peaks in the cathodic region related to the conversions of the reduction of the anodic peaks [27–30]. In Fig. 4b, three characteristic nickel peaks can be seen. These peaks correspond to the transformations of Ni/Ni^{II}, Ni^{II}/Ni^{III}

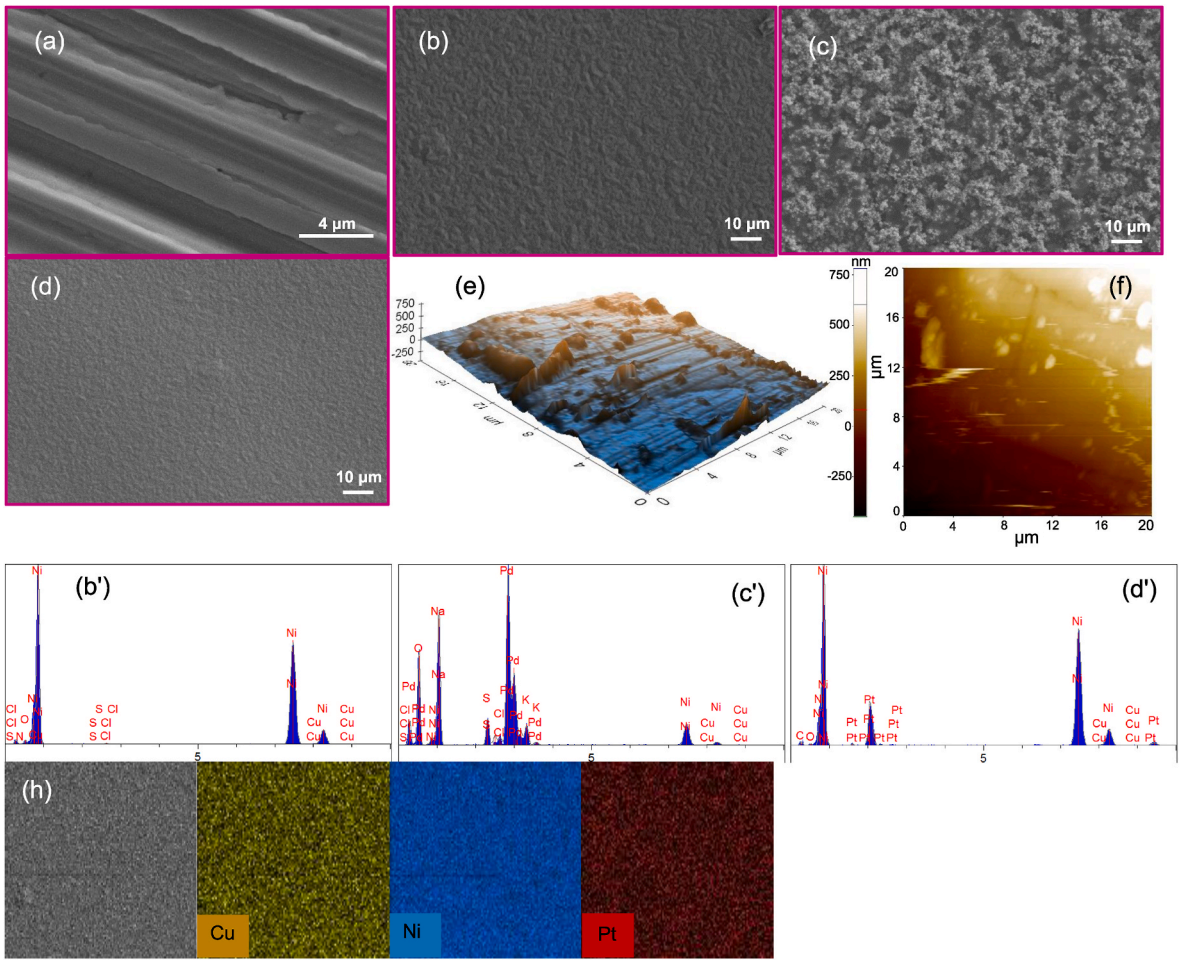

Fig. 1. SEM images (a,b,c,d,h) and EDX spectrums (b',c',d') of polished Cu (a), Cu/Ni (b,b'), Cu/Ni–Pd (c,c'), and Cu/Ni–Pt (d,d',h). 3D (e) and 2D (f) AFM images of Cu/Ni–Pt. EDX mapping of Cu/Ni–Pt. Magnification of SEM images is 1000 X.

Table 1
EDX data of prepared electrocatalysts.

Coating	Atomic%				
	Cu	Ni	Pt	Pd	Others
Cu/Ni	0.61	88.99	–	–	10.40
Cu/Ni–Pd	0.22	10.62	–	42.38	46.78
Cu/Ni–Pt	0.70	76.24	17.72	–	5.34

in the anodic region and Ni^{III}/Ni^{II} in the cathodic region [31]. As with Cu/Ni–Pd, a broad peak at −0.356 V vs RHE corresponds to hydrogen desorption superimposed by the formation of a Pd oxide layer. The reduction of Pd^{II}/Pd is observed at −0.255 V vs RHE [32,33]. Conversions of Ni^{II}/Ni^{III} and Ni^{III}/Ni^{II} are also seen. In Fig. 4d, it is clearly seen that individual platinum atoms are deposited on the Cu/Ni surface. The electrocatalytic properties of the prepared electrodes are shown in Fig. 4 and the collected data in Table 2. The initial hydrogen adsorption/desorption potentials are −1.313 [10], −1.284, −1.129 and −0.864 V vs RHE for Cu, Cu/Ni, Cu/Ni–Pd and Cu/Ni–Pt, respectively (Fig. 4e). The lowest hydrogen overpotential is obtained for Cu/Ni–Pt. Fig. 4f shows the LSV curves prepared electocatalysts in 1.0 M KOH solution. Comparing LSV curves of HER on the surface of Cu, Cu/Ni, Cu/Ni–Pd and Cu/Ni–Pt, it can be seen that a small amount of Pt on the Ni coating increases the current density values. Exchange current density (i_o) and Tafel slope (b_c) giving in Table 2 are determined via Tafel extrapolating method. These parameters could not be calculated for Cu and Cu/Ni due to observing oxygen evolution. In order to make a reliable comparison between all electrodes, current density at specific overpotentials (−1.05, −1.15 and −1.25 V vs RHE) is also obtained and is given in Table 2. Pd and Pt modified electrocatalysts have higher current densities at the specific overpotentials in comparison with bare Cu and Cu/Ni. One of the significant performance metrics for HER electrocatalysts is the exchange current density. Although high overpotential (862 mV) at 10 mA cm^{-2} is measured on Cu/Ni–Pt, very high exchange current density with 5.65 mA cm^{-2} is obtained on Cu/Ni–Pt. When compared to literature results containing Ni and Pt electrocatalysts in terms of exchange current density, for example, Pierozynski and Mikolajczyk reported the HER behavior of platinum-modified nickel foam catalyst in 0.1 M NaOH solution. They found the exchange current density as 0.054 mA cm^{-2} [34]. Mosallanezhad et al. prepared the f Pt@CoS catalyst and performance of this catalyst was studied in 1.0 M KOH solution to determine the HER activity. Exchange current density was found to be 2.20 mA cm^{-2}. Besides, they found the i_o of Pt/C as 1.73 mA cm^{-2} [35]. Feng' s group was prepared the nickel nanowire arrays ((111), (200) and (220) lattice planes) as HER catalysts on a titanium sheet using electrodeposition method. They stated that $Ni_{(220)}$ had a high j_o (151 μA cm^{-2}) and was larger than that of the others [36]. Hussain et al. investigated the platinum (Pt) based dichalcogenides (PtS_2, $PtSe_2$ and $PtTe_2$) as highly energetic and robust hydrogen evolution electrocatalysts. The highest exchange current density with 0.81 mA cm^{-2} was obtained on $PtTe_2$ in basic electrolyte [37]. Shi et al. were successfully synthesized the PtFe nanofoams with face center cubic (fcc) phase. While they found the exchange current density of commercial Pt/C as 3.2 mA cm^{-2}, i_o of synthesized PtFe-mix found to be 3.6 mA cm^{-2} [38]. Zhang of research

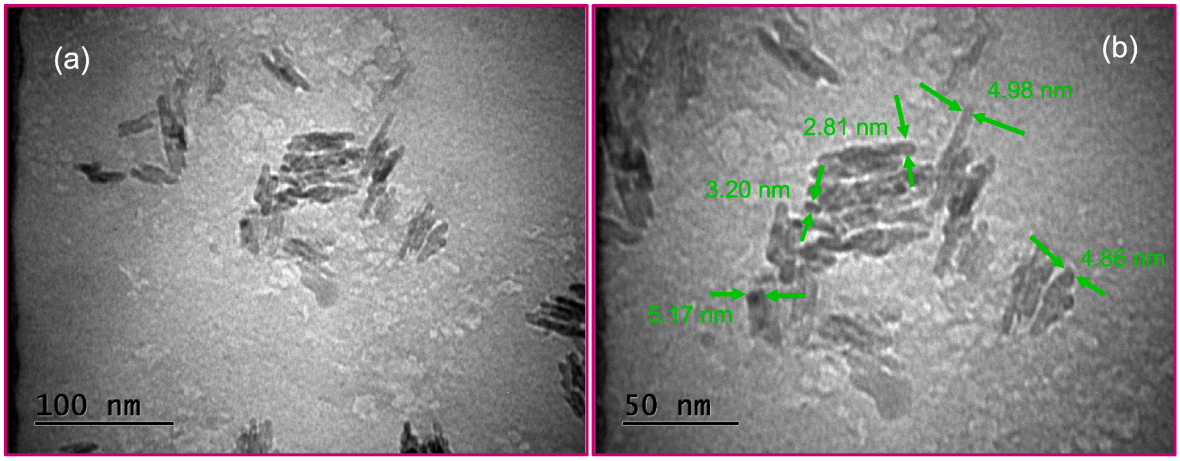

Fig. 2. TEM (a) and HRTEM (b) images of Cu/Ni–Pt.

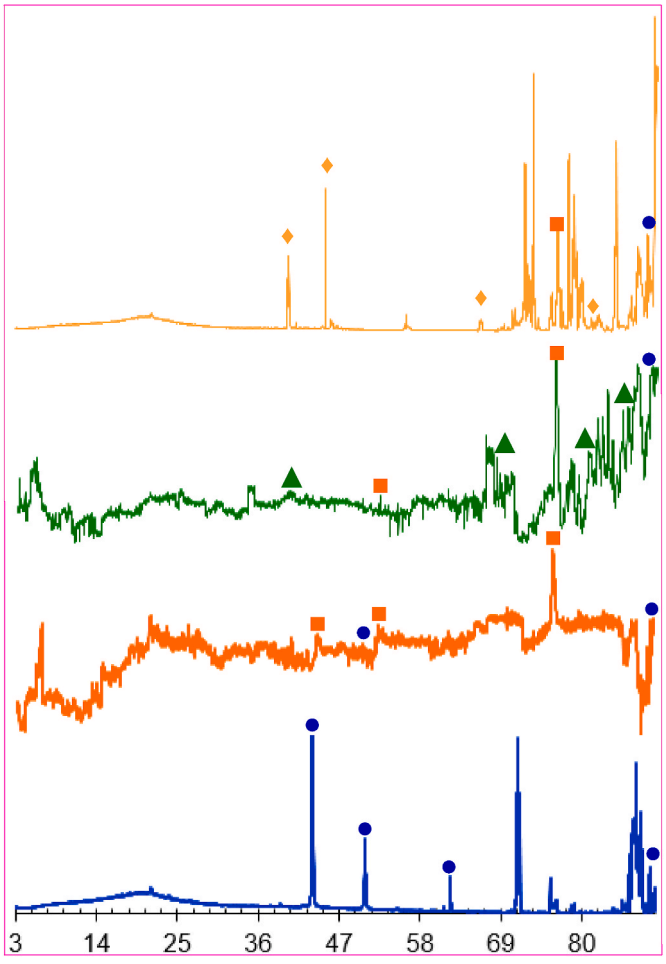

Fig. 3. XRD patterns of prepared electrocatalysts (♦: Pt, ▲: Pd, ■: Ni, ●: Cu).

team produced a Ni–Fe electrocatalysts on Ni foam which has the exchange current density with 0.852 mA cm^{-2} in 1 M KOH solution [39]. Electrochemical synthesis of Ni–Rh and Co–Ni–Rh thin layers has been reported by Kutyła et al. This group found very high exchange current density (17.102 mA cm^{-2}) among our investigations [40]. Yu et al. was fabrication of a porous Ni–Cu alloy as cathode to use in the process of hydrogen evolution reaction. In this study, the value of i_o was 2.24x10^{-3} mA cm^{-2} [41]. As discussed above, the Cu/Ni–Pt electrocatalyst performs better than the most of the nickel and platinum-containing HER catalysts reported so far, in terms of exchange current density against alkaline HER. This high activity can depend on i) it is well-known high intrinsic electrocatalytic property of Pt, ii) high surface area, iii) high active sites, iv) encouraging the production of oxyl or hydroxyl radicals and v) changing electronic structure (synergistic effect) [13,42,43]. In addition to exchange current density, another significant performance metric is Tafel slope exhibiting about HER kinetic mechanism. Under alkaline conditions, well-known HER kinetic mechanism as follows: Electrochemical adsorption step is the first step as known Volmer reaction, containing the forming hydrogen intermediate (H*) (~120 mV dec^{-1}). After Volmer step, there are two reactions going on competitively. One is Heyrovsky reaction consisting of electrochemical desorption step of H_2 (~40 mV dec^{-1}) and the second as known Tafel reaction which is chemical desorption step (~30 mV dec^{-1}). HER kinetic mechanism goes on combination of these reactions [44]. In this study, Tafel slopes of Cu/Ni–Pt and Cu/Ni–Pd electrocatalysts are found to be 133 and 187 mV dec^{-1}, respectively. Tafel slope of Cu/Ni–Pt is smaller than that of Pd modified and HER kinetic mechanism moves on Volmer reaction. EIS measurements are employed to further confirm the electroactivity of Cu/Ni–Pt and to investigate the interfacial charge transfer kinetics. Fig. 4g and h illustrate the Nyquist and Bode plots of prepared electrocatalysts at −1.15 V (vs RHE). These spectra are fitted by a Zview2 software using Randles circuit model (Fig. 4i as inset) and corresponding circuit elements are summarized in Table 2. Not ideal one semicircular section is appeared for all prepared electrocatalysts. One semicircular section points out charge transfer for the HER [45]. Faster charge transfer kinetics is equal to lower charge transfer resistance (R_{ct}) [46]. While very high R_{ct} values are obtained on bare Cu and Cu/Ni, Cu/Ni–Pt shows very small R_{ct} values at different overpotentials more improving the charge transfer kinetics. On the other hand, as the overpotentials increase, R_{ct} values decrease as shown in Fig. 4i and Table 2. Improved catalyst must have a notable long-term stability under alkaline conditions for industrialization. Therefore, chronoamperometrical approach is used to investigate long-term behavior of Cu/Ni–Pt, as given in Fig. 4j. Measured current densities are found to be −115 mA cm^{-2} at the beginning, −101 mA cm^{-2} at the 2.5th h and −108 mA cm^{-2} at the end of 4 h. One another stability test is cyclic stability. Fig. 4k presents the cyclic stability test of Cu/Ni–Pt in 1.0 M KOH. Potential differences are found to be 10 and 50 mV at current densities of 10 and 50 mA cm^{-2}, respectively. Since there is not a significant current density decay and shifting in the potential over 4 h and after 400 cycles on this electrocatalyst. It is suggested that developed electrocatalyst is suitable for long-term applications in industrial.

Since commercial electrolyzers operate in the long term, corrosion is

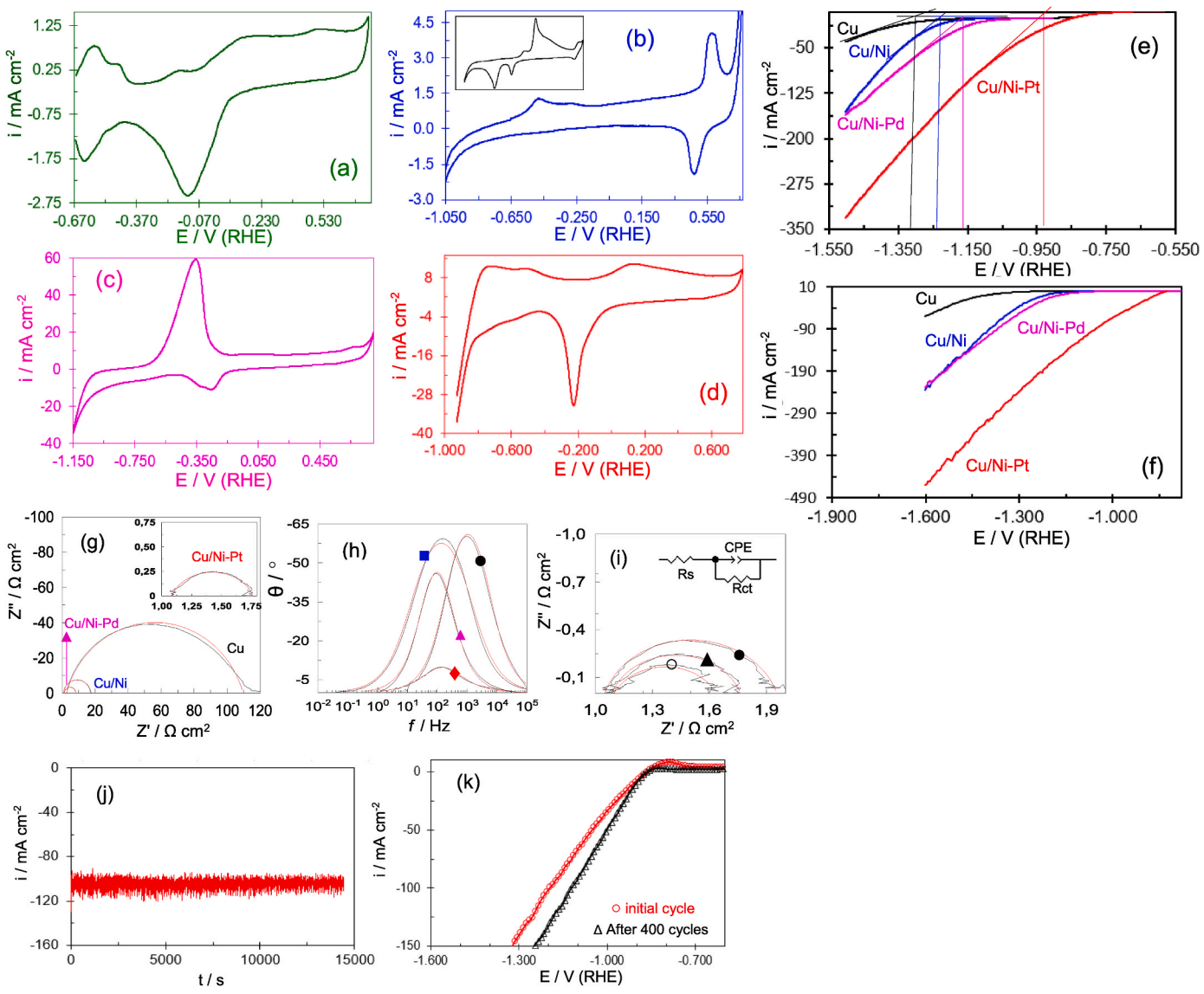

Fig. 4. Cyclic voltammograms of Pt (a), Cu (as inset in b), Cu/Ni (b), Cu/Ni–Pd (c) and Cu/Ni–Pt (d) at 100 mV s^{-1}. Hydrogen adsorption region of cyclic voltammograms (e). Cathodic current-potential curves (f) and Nyquist plots (g) at −1.15 V (vs RHE) of electrocatalysts and Nyquist plots (i) of Cu/Ni–Pt at −1.05 (●), −1.15 (▲) and −1.25 V (○) (vs RHE). Bode plots (h) of Cu (●), Cu/Ni (■), Cu/Ni–Pd (▲) and Cu/Ni–Pt (♦). Equivalent circuit model is given as inset in i for all electrocatalysts. Red straight lines show fitting curves for g-i. Chronoamperometric curve (j) of Cu/Ni–Pt at −1.25 V (vs RHE). Cycle test (k) of Cu/Ni–Pt at a scan rate of 50 mV s^{-1}. All experiments are carried out in 1.0 M KOH solution. (For interpretation of the references to colour in this figure legend, the reader is referred to the Web version of this article.)

Table 2
Electrochemical data obtained from cathodic current-potential curves and EIS of prepared electrocatalysts.

Electrocatalyst	b_c/mV dec^{-1}	i_o/mA cm^{-2}	-η/V	*CPE* (10^{-3}) $Y_o/s^n\ \Omega^{-1}\ cm^{-2}$	*n*	R_{ct}/Ω cm^2	*i*/mA cm^{-2}
Cu	–	–	1.05	2.05	0.71	652.0	0.14
			1.15	0.24	0.82	107.0	0.39
			1.25	0.12	0.89	29.0	1.31
Cu/Ni	–	–	1.05	0.10	0.94	80.37	0.39
			1.15	7.00	0.94	16.41	0.77
			1.25	0.07	0.94	9.34	18.76
Cu/Ni–Pd	187	0.045	1.05	1.17	0.92	42.17	1.34
			1.15	0.74	0.97	7.10	7.35
			1.25	0.84	0.94	1.30	32.12
Cu/Ni–Pt	133	5.650	1.05	8.06	0.81	0.91	88.62
			1.15	8.70	0.79	0.68	144.73
			1.25	12.92	0.70	0.54	205.02

a quite important parameter for the life of the electrolyzers. Most scientists ignore determining the corrosion behavior of the catalysts they prepare. However, corrosion directly affects catalytic activity. Therefore, in this study, in addition to catalytic activity and long-time stability experiments, the corrosion behavior of Cu/Ni–Pt was examined in detail in alkaline media. To evaluate the corrosion performance of Cu/Ni–Pt, anodic current-potential curves and EIS are taken at the open circuit potential (E_{ocp}). Nyquist and Bode diagrams and anodic current-potential curves of Cu/Ni–Pt are shown in Fig. 5. The EIS results are also fitted using Zview2 software and the equivalent circuit with the two-time constant, which can be seen in the Bode diagrams, is shown in Fig. 5c. Not ideal small semicircular section at high frequency is related to the charge transfer resistance (R_{ct}), diffuse layer resistance (R_d) and capacitance (R2-CPE1, R2=R_{ct} + R_d) and not ideal large semicircular section not closed at low frequency indicate the passivated layer (oxide film) resistance and capacitance (R3-CPE2). Polarization resistance (R_p) is sum of R2 and R3. In the fitting, constant phase element (CPE) is used instead of double layer capacitance (C_{dl}) since this system is not ideal capacitor. From the Nyquist diagrams, the polarization resistances after 24, 48, 72, 120 and 144 h of exposure to 1.0 M KOH solution are 2158, 4412, 4486, 4306 and 6880 Ω cm^2, respectively. As exposure time increases, in general, R_p values increase because much more corrosion products form on the surface [41,47]. To learn anodic behavior of Cu/Ni–Pt, this surface is polarized with the beginning from E_{ocp} to 1.2 V vs RHE, as given in Fig. 5d. As can be seen in Fig. 5d, passivated layer where the current density does not change forms [48,49]. This layer prevents to attack aggressive ions throughout the surface, resulting in an improvement in corrosion resistance [50]. Hence, it can be said that Cu/Ni–Pt has excellent properties in terms of electrocatalysis and corrosion resistance.

4. Conclusions

In summary, to determine the two properties, HER and corrosion resistance, of the Cu/Ni–Pt electrode was equiped through a one-step electrodeposition method. Nickel, copper, palladium and platinum peaks are clearly seen in EDX and XRD spectrums on the surface. TEM showed the dispersion of Pt atoms over the Cu/Ni surface. High exchange current density with 5.65 mA cm^{-2} was measured on Cu/Ni–Pt. While very high R_{ct} values are obtained on bare Cu and Cu/Ni, Cu/Ni–Pt shows very small R_{ct} values at different overpotentials more improving the charge transfer kinetics. Enhanced activity was explained based on it is well-known high intrinsic electrocatalytic property of Pt, high surface area, high active sites, encouraging the production of oxyl or hydroxyl radicals and synergistic effect. Besides, HER property of Cu/Ni-Pt electrode is compared with literature data in terms of exchange current density and well discussed. The CA and cyclic stability data of the Cu/Ni–Pt showed a good long-term stability over 4 h and after 400 cycles. The dispersion of Pt nanoparticles over the Cu/Ni surface increased the HER and the anti-corrosion properties. The high anti-corrosion property is by virtue of the occurrence of a preventive passive layer with time.

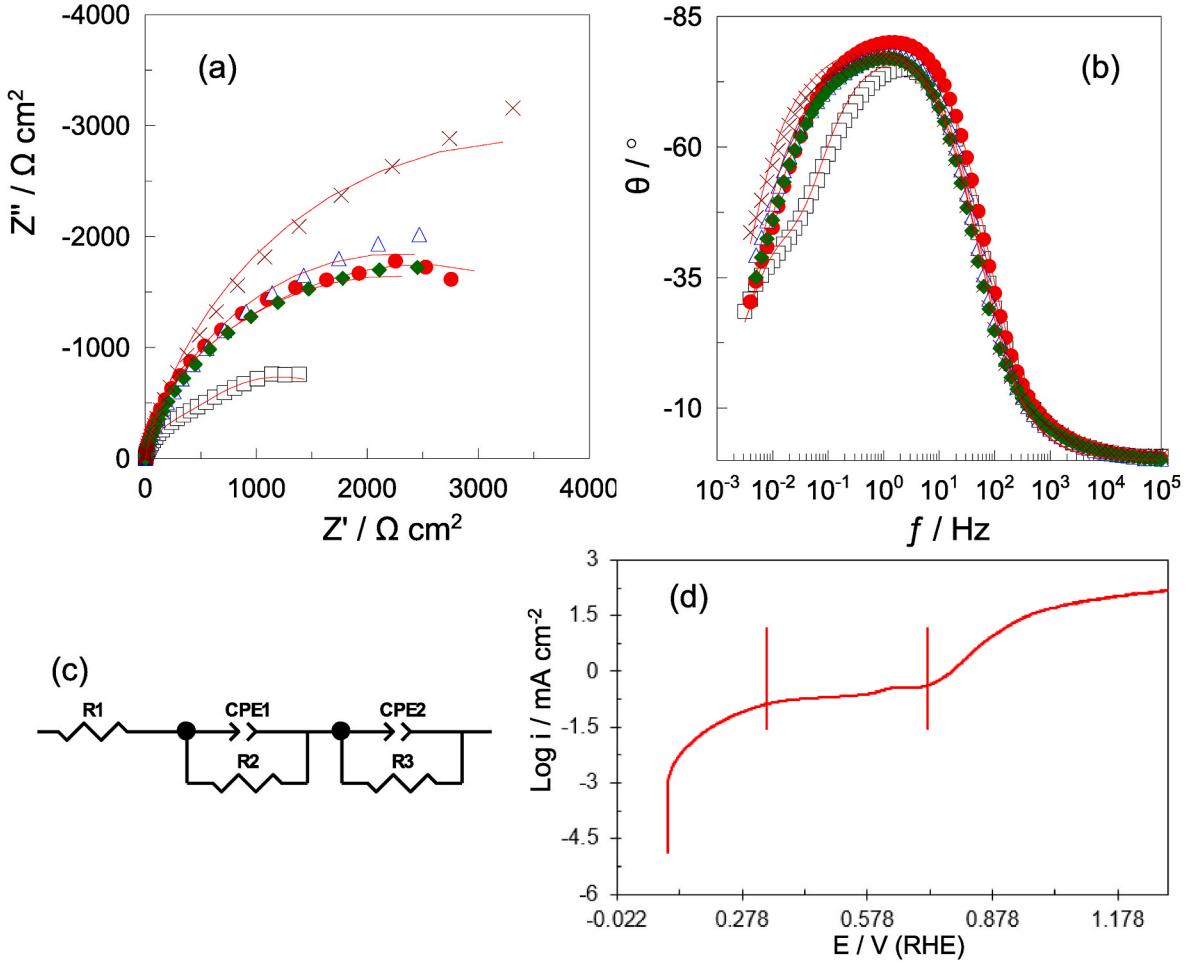

Fig. 5. Nyquist (a) and Bode (b) plots of Cu/Ni–Pt after 24 (□), 48 (●), 72 (△), 120 (♦) and 144 (x) h exposure times. Equivalent circuit model for Nyquist and Bode plots (c) and anodic current-potential curves (d) of Cu/Ni–Pt after 144 h exposure time. Red straight lines show fitting curves for a and b. All experiments are carried out in 1.0 M KOH solution. (For interpretation of the references to colour in this figure legend, the reader is referred to the Web version of this article.)

Declaration of competing interest

We declare that,

The article is original, has been written by the stated authors who are all aware of its content and approve its submission, no conflict of interest exists, or if such conflict exists, the exact nature of the conflict must be declared and if accepted, it will not be published elsewhere in the same form, in English or in any other language, without the written consent of the Publisher.

Acknowledgements

We would like to thank to Mardin Artuklu University for this opportunity. The authors are very grateful to Prof. Dr. Reşit YILDIZ from Mardin Artuklu University for his contributions.

References

[1] Zhan G, Yao Y, Quan F, Gu H, Liu X, Zhang L. D-band frontier: a new hydrogen evolution reaction activity descriptor of Pt single-atom catalysts. J Energy Chem 2022;72:203–9. https://doi.org/10.1016/j.jechem.2022.05.012.

[2] Gopinath M, Marimuthu R. A review on solar energy-based indirect water-splitting methods for hydrogen generation. Int J Hydrogen Energy 2022;47:37742–59. https://doi.org/10.1016/j.ijhydene.2022.08.297.

[3] Gao Q, Zhang W, Shi Z, Yang L, Tang Y. Structural design and electronic modulation of transition metal-carbide electrocatalysts toward efficient hydrogen evolution. Adv Mater 2019;31:1802880. https://doi.org/10.1002/adma.201802880.

[4] Seh ZW, Kibsgaard J, Dickens CF, Chorkendorff IB, Nørskov JK, Jaramillo TF. Combining theory and experiment in electrocatalysis: insights into materials design. Science 2017;355(6321). https://doi.org/10.1126/science.aad4998.

[5] Wang J, Wei Z, Mao S, Li H, Wang Y. Highly uniform Ru nanoparticles over N-doped carbon: pH and temperature-universal hydrogen release from water reduction. Energy Environ Sci 2018;11:800–6. https://doi.org/10.1039/C7EE03345A.

[6] Zheng Y, Jiao Y, Jaroniec M, Qiao SZ. Advancing the electrochemistry of the hydrogen-evolution reaction through combining experiment and theory. Angew Chem Int Ed 2015;54:52–65. https://doi.org/10.1002/anie.201407031.

[7] Anantharaj S, Karthik PE, Subramanian B, Kundu S. Pt nanoparticle anchored molecular self-assemblies of DNA: an extremely stable and efficient HER electrocatalyst with ultralow Pt content. ACS Catal 2016;6:4660–72. https://doi.org/10.1021/acscatal.6b00965.

[8] Solmaz R, Döner A, Kardaş G. The stability of hydrogen evolution activity and corrosion behavior of NiCu coatings with long-term electrolysis in alkaline solution. Int J Hydrogen Energy 2009;34:2089–94. https://doi.org/10.1016/j.ijhydene.2009.01.007.

[9] Solmaz R, Döner A, Şahin İ, Yüce AO, Kardaş G, Yazıcı B, Erbil M. The stability of NiCoZn electrocatalyst for hydrogen evolution activity in alkaline solution during long-term electrolysis. Int J Hydrogen Energy 2009;34:7910–8. https://doi.org/10.1016/j.ijhydene.2009.07.086.

[10] Döner A, Toprak Döşlü S. Pt modified copper coated copper as an efficient electrocatalyst for hydrogen evolution. International world energy conference II. Proceeding Book; 2022. p. 12–8.

[11] Huang L, Wei M, Zaman S, Ali A, Xia BY. Well-connection of micro-platinum and cobalt oxide flower array with optimized water dissociation and hydrogen recombination for efficient overall water splitting. Chem Eng J 2020;398:125669. https://doi.org/10.1016/j.cej.2020.125669.

[12] Mojabi S, Sanjabi S. Decorated fractal Ni-Cu foam with Pd nanoparticles as a high-performance electrocatalyst toward hydrogen evolution reaction. Thin Solid Films 2022;758:139415. https://doi.org/10.1016/j.tsf.2022.139415.

[13] Chauhan N, Choi HW, Kumar M, Yoon D. Nanoarchitectonics Pt/NiCo in a carbon matrix as highly efficient electrocatalyst for hydrogen evolution reaction. Electrochim Acta 2023;460:142634. https://doi.org/10.1016/j.electacta.2023.142634.

[14] Guo X, Wan X, Liu Q, Li Y, Li W, Shui J. Phosphated IrMo bimetallic cluster for efficient hydrogen evolution reaction. eScience 2022;2:304–10. https://doi.org/10.1016/j.esci.2022.04.002.

[15] Li C, Zhao X, Liu Y, Wei W, Lin Y. 3D Ni-Co sulfoxide nanosheet arrays electrodeposited on Ni foam: a bifunctional electrocatalyst towards efficient and stable water splitting. Electrochim Acta 2018;292:347–56. https://doi.org/10.1016/j.electacta.2018.06.159.

[16] Liu X, Zhu S, Liang Y, Jiang H, Li Z, Wu S, Cui Z. Self-standing nanoporous NiPd bimetallic electrocatalysts with ultra-low Pd loading for efficient hydrogen evolution reaction. Electrochim Acta 2022;41:140077. https://doi.org/10.1016/j.electacta.2022.140077.

[17] Wang S, Li N, Liu L. Enhanced hydrogen generation performance of Pd-based micro/nano hierarchical porous structure. Mater Lett 2018;228:443–6. https://doi.org/10.1016/j.matlet.2018.06.090.

[18] Cardoso JASB, Šljukić B, Kayhan E, Sequeira CAC, Santos DMF. Palladium-nickel on tin oxide-carbon composite supports for electrocatalytic hydrogen evolution. Catal Today 2020;357:302–10. https://doi.org/10.1016/j.cattod.2019.05.056.

[19] Ehsan MA, Suliman MH, Rehman A, Hakeem AS, Ghanim AA, Qamar M. Fabrication of platinum thin films for ultra-high electrocatalytic hydrogen evolution reaction. Int J Hydrogen Energy 2020;45:15076–85. https://doi.org/10.1016/j.ijhydene.2020.03.218.

[20] Liu Y, Hangarter CM, Garcia D, Moffat TP. Self-terminating electrodeposition of ultrathin Pt films on Ni: an active, low-cost electrode for H_2 production. Surf Sci 2015;631:141–54. https://doi.org/10.1016/j.susc.2014.06.002.

[21] Eiler K, Fornell J, Navarro-Senent C, Pellicer E, Sort J. Tailoring magnetic and mechanical properties of mesoporous single-phase Ni–Pt films by electrodeposition. Nanoscale 2020;12:7749–58. https://doi.org/10.1039/C9NR10757F.

[22] Guo Y, Chang X, Fu K, Zheng X, Zheng J, Li X. Amorphous Ni/C nanocomposites from tandem plasma reaction for hydrogen evolution. Int J Hydrogen Energy 2019;44:18115–22. https://doi.org/10.1016/j.ijhydene.2019.04.246.

[23] Papandrewa AB, Zawodzinski Jr TA. Nickel catalysts for hydrogen evolution from CsH_2PO_4. J Power Sources 2014;245:171–4. https://doi.org/10.1016/j.jpowsour.2013.06.141.

[24] Chen M, Lou B, Ni Z, Xu B. PtCo nanoparticles supported on expanded graphite as electrocatalyst for direct methanol fuel cell. Electrochim Acta 2015;165:105–9. https://doi.org/10.1016/j.electacta.2015.03.007.

[25] Shaik MR, Ali ZJQ, Khan M, Kuniyil M, Assal ME, Alkhathlan HZ, Al-Warthan A, Siddiqui MRH, Khan M, Adil SF. Green synthesis and characterization of palladium nanoparticles using origanum vulgare L. Extract and their catalytic activity. Molecules 2017;22:165. https://doi.org/10.3390/molecules22010165.

[26] Bharate BG. Nanocubes of palladium, simple, green approach and catalytic properties under continuous hydrogenation system. Biomed J Sci Tech Res 2019;19:14672–5. https://doi.org/10.26717/BJSTR.2019.19.003375.

[27] Pyun CH, Park SM. Insitu spectroelectrochemical studies on anodic-oxidation of copper in alkaline-solution. J Electrochem Soc 1986;133:2024–30. https://doi.org/10.1149/1.2108333.

[28] Burke LD, Collins JA. Role of surface defects in the electrocatalytic behaviour of copper in base. J Appl Electrochem 1999;29:1427–38. https://doi.org/10.1023/A:1003805008453.

[29] Abd el Haleem SM, Ateya BG. Cyclic voltammetry of copper in sodium hydroxide solutions. J Electroanal Chem 1981;117:309–19. https://doi.org/10.1016/S0022-0728(81)80091-5.

[30] Burke LD, Collins JA, Murphy MA. Redox and electrocatalytic activity of copper in base at unusually low, premonolayer potentials. J Solid State Electrochem 1999;4:34–41. https://doi.org/10.1007/s100080050189.

[31] Vukovic M. Voltammetry and anodic stability of a hydrous oxide film on a nickel electrode in alkaline solution. J Appl Electrochem 1994;24. https://doi.org/10.1007/BF00348775. 878-82.

[32] Bolzan AE. Phenomenological aspects related to the electrochemical behavior of smooth palladium electrodes in alkaline solutions. J Electroanal Chem 1995;380. https://doi.org/10.1016/0022-0728(94)03627-F. 127-38.

[33] Cai J, Huang Y, Guo Y. Bi-modified Pd/C catalyst via irreversible adsorption and its catalytic activity for ethanol oxidation in alkaline medium. Electrochim Acta 2013;99:22–9. https://doi.org/10.1016/j.electacta.2013.03.059.

[34] Pierozynski B, Mikolajczyk T. Cathodic evolution of hydrogen on platinum-modified nickel foam catalyst. Electrocatalysis 2016;7:121–6. https://doi.org/10.1007/s12678-015-0290-x.

[35] Amirabbas M, Cong W, Payam AK, Yanyan F, Shuwen N, Zenan B, Bo L, Ting H, Hongge P, Gongming W. Interfacial synergies between single-atomic Pt and CoS for enhancing hydrogen evolution reaction catalysis. Appl Catal B 2022;315:121534. https://doi.org/10.1016/j.apcatb.2022.121534.

[36] Feng X, Bian S, Wang N, Wang F, Guan H, Hao X, Ma M, Gao X, Chenz Y. Nickel nanowire arrays with preferential orientation for boosting hydrogen evolution reaction capability. J Electrochem Soc 2020;167:106501. https://doi.org/10.1149/1945-7111/ab9756.

[37] Hussain S, Akbar K, Vikraman D, Rabani I, Song W, Ki-Seok An, Hyun-Seok K, Seung-Hyun C, Jung J. Experimental and theoretical insights to demonstrate the hydrogen evolution activity of layered platinum dichalcogenides electrocatalysts. J Mater Res Technol 2021;12:385–98. https://doi.org/10.1016/j.jmrt.2021.02.097.

[38] Shi Y, Zhang D, Huang H, Miao H, Wu X, Zhao H, Zhan T, Chen X, Lai J, Wang L. Mixture phases engineering of PtFe nanofoams for efficient hydrogen evolution. Small 2022;18:2106947. https://doi.org/10.1002/smll.202106947.

[39] Zhang Z, Wu Y, Zhang D. Potentiostatic electrodeposition of cost-effective and efficient Ni-Fe electrocatalysts on Ni foam for the alkaline hydrogen evolution reaction. Int J Hydrogen Energy 2022;47:1425–34. https://doi.org/10.1016/j.ijhydene.2021.10.150.

[40] Kutyła D, Salcı A, Kwiecinska A, Kołczyk-Siedlecka K, Kowalik R, Zabinski P, Solmaz R. Catalytic activity of electrodeposited ternary Co-Ni-Rh thin films for water splitting process. Int J Hydrogen Energy 2020;45:34805–17. https://doi.org/10.1016/j.ijhydene.2020.05.196.

[41] Yu L, Lei T, Nan B, Jiang Y, He Y, Liu CT. Characteristics of a sintered porous Ni-Cu alloy cathode for hydrogen production in a potassium hydroxide solution. Energy 2016;97:498–505. https://doi.org/10.1016/j.energy.2015.12.138.

[42] Kim T, Roy SB, Moon S, Yoo S, Choi H, Parale VG, Kim Y, Lee J, Jun SC, Kang K, Chun SH, Kanamori K, Park HH. Highly dispersed Pt clusters on F-Doped Tin(IV) oxide aerogel matrix: an ultra-robust hybrid catalyst for enhanced hydrogen evolution. ACS Nano 2022;16:1625–38. https://doi.org/10.1021/acsnano.1c10504.

[43] Battiato S, Bruno L, Terrasi A, Mirabella S. Superior performances of electroless-deposited Ni–P films decorated with an ultralow content of Pt for water-splitting

reactions. ACS Appl Energy Mater 2022;5:2391–9. https://doi.org/10.1021/acsaem.1c03880.

[44] Yang Y, Yu Y, Li J, Chen Q, Du Y, Rao P, Li R, Jia C, Kang Z, Deng P, Shen Y, Tian X. Engineering ruthenium-based electrocatalysts for effective hydrogen evolution reaction. Nano-Micro Lett 2021;13:160. https://doi.org/10.1007/s40820-021-00679-3.

[45] Adam YS, Telli E, Farsak M, Kardaş G. Hydrogen production activity of nickel deposited graphite electrodes doped with CoW and CoIr nanoparticles. Int J Hydrogen Energy 2023;48:31844–54. https://doi.org/10.1016/j.ijhydene.2023.04.344.

[46] Chen Y, Li J, Wang N, Zhou Y, Zheng J, Chu W. Plasma-assisted highly dispersed Pt single atoms on Ru nanoclusters electrocatalyst for pH-universal hydrogen evolution. Chem Eng J 2022;48:137611. https://doi.org/10.1016/j.cej.2022.137611.

[47] Sherif El-Sayed M, Erasmus RM, Comins JD. Corrosion of copper in aerated synthetic sea water solutions and its inhibition by 3-amino-1,2,4-triazole. J Colloid Interface Sci 2007;309:470–7. https://doi.org/10.1016/j.jcis.2007.01.003.

[48] Kong J, Sabatini M, Monaco L, Tam J, McCrea JL, Palumbo G, Howe J, Erb U. Characterization of a nanocrystalline NiCo electroformed sheet metal. J Mater Sci 2021;56:1749–67. https://doi.org/10.1007/s10853-020-05325-8.

[49] Tang J, Zhao X, Zuo Y, Ju P, Tang Y. Electrodeposited Pd-Ni-Mo film as a cathode material for hydrogen evolution reaction. Electrochim Acta 2015;174:1041–9. https://doi.org/10.1016/j.electacta.2015.06.134.

[50] Khorsand S, Raeissi K, Ashrafizadeh F. Corrosion resistance and long-term durability of super-hydrophobicnickel film prepared by electrodeposition process. Appl Surf Sci 2014;305:498–505. https://doi.org/10.1016/j.apsusc.2014.03.123.